Physics Letters B 768 (2017) 387–392

Contents lists available at ScienceDirect

Physics Letters B

www.elsevier.com/locate/physletb

Observation of isoscalar and isovector dipole excitations in neutron-rich ^{20}O

N. Nakatsuka [a,b,*], H. Baba [b], T. Aumann [c,d], R. Avigo [e,f], S.R. Banerjee [g], A. Bracco [e,f], C. Caesar [c,d], F. Camera [e,f], S. Ceruti [e,f], S. Chen [h,b], V. Derya [i], P. Doornenbal [b], A. Giaz [e,f], A. Horvat [c,d], K. Ieki [j], T. Inakura [k], N. Imai [l], T. Kawabata [a], N. Kobayashi [m], Y. Kondo [n], S. Koyama [m], M. Kurata-Nishimura [b], S. Masuoka [l], M. Matsushita [l], S. Michimasa [l], B. Million [e], T. Motobayashi [b], T. Murakami [a], T. Nakamura [n], T. Ohnishi [b], H.J. Ong [o], S. Ota [l], H. Otsu [b], T. Ozaki [n], A. Saito [n], H. Sakurai [m,b], H. Scheit [c], F. Schindler [c,d], P. Schrock [c], Y. Shiga [j,b], M. Shikata [n], S. Shimoura [l], D. Steppenbeck [b], T. Sumikama [b], I. Syndikus [c,d], H. Takeda [b], S. Takeuchi [b], A. Tamii [o], R. Taniuchi [m], Y. Togano [n], J. Tscheuschner [c], J. Tsubota [n], H. Wang [b], O. Wieland [e], K. Wimmer [m], Y. Yamaguchi [l], K. Yoneda [b], J. Zenihiro [b]

[a] Department of Physics, Kyoto University, Kyoto 606-8502, Japan
[b] RIKEN Nishina Center, Saitama 351-0198, Japan
[c] Institut für Kernphysik, Technische Universität Darmstadt, D-64289 Darmstadt, Germany
[d] GSI Helmholtzzentrum für Schwerionenforschung GmbH, D-64291 Darmstadt, Germany
[e] INFN Sezione di Milano, I-20133 Milano, Italy
[f] Dipartimento di Fisica dell'Università degli Studi di Milano, I-20133 Milano, Italy
[g] Variable Energy Cyclotron Centre, 1/AF, Bidhannagar, Kolkata, 700064, India
[h] School of Physics and State Key Laboratory of Nuclear Physics and Technology, Peking University, Beijing 100871, China
[i] Institut für Kernphysik, Universität zu Köln, D-50937 Köln, Germany
[j] Department of Physics, Rikkyo University, Tokyo 171-8501, Japan
[k] Department of Physics, Niigata University, Niigata 950-2181, Japan
[l] Center for Nuclear Study, The University of Tokyo, Tokyo 113-0033, Japan
[m] Department of Physics, The University of Tokyo, Tokyo 113-0033, Japan
[n] Department of Physics, Tokyo Institute of Technology, Tokyo 152-8551, Japan
[o] Research Center for Nuclear Physics, Osaka University, Osaka 567-0047, Japan

ARTICLE INFO

Article history:
Received 10 February 2017
Received in revised form 1 March 2017
Accepted 8 March 2017
Available online 14 March 2017
Editor: V. Metag

Keywords:
^{20}O
Low-energy dipole excitation
Inelastic α scattering
Virtual-photon excitation

ABSTRACT

The isospin characters of low-energy dipole excitations in neutron-rich unstable nucleus ^{20}O were investigated, for the first time in unstable nuclei. Two spectra obtained from a dominant isovector probe (^{20}O + Au) and a dominant isoscalar probe (^{20}O + α) were compared and analyzed by the distorted-wave Born approximation to extract independently the isovector and isoscalar dipole strengths. Two known 1^- states with large isovector dipole strengths at energies of 5.36(5) MeV (1^-_1) and 6.84(7) MeV (1^-_2) were also excited by the isoscalar probe. These two states were found to have different isoscalar dipole strengths, 2.70(32)% (1^-_1) and 0.67(12)% (1^-_2), respectively, in exhaustion of the isoscalar dipole-energy-weighted sum rule. The difference in isoscalar strength indicated that they have different underlying structures.

* Corresponding author at: Department of Physics, Kyoto University, Kyoto 606-8502, Japan.
E-mail address: nakatsuka@scphys.kyoto-u.ac.jp (N. Nakatsuka).

http://dx.doi.org/10.1016/j.physletb.2017.03.017

1. Introduction

The electric dipole response, or $E1$ response, is one of the most interesting properties of atomic nuclei. In medium to heavy neutron-rich nuclei, the electric dipole excitation is fragmented into a low-energy region around the neutron separation energy [1–3]. These low-energy dipole excitations, or so-called Pygmy dipole resonance, are of great interest, since they can have significant cross sections in photo-absorption reactions, and thus, have an impact on astrophysical phenomena, such as r-process nucleosynthesis.

Following an early study on a set of stable magic nuclei [4,5], recent experimental studies on ^{40,48}Ca [6], ^{74}Ge [7], ^{124}Sn [8], ^{138}Ba [9], and ^{140}Ce [9,10] have demonstrated that low-energy dipole excitations exhibit a specific isospin character, sometimes referred to as "isospin splitting". These experiments compared the dipole excitations populated by two probes: the inelastic scattering of alpha particles, populated by a dominant isoscalar probe, and real photon scattering, populated by a dominant isovector probe. They revealed that some dipole excitations, mostly in the low-energy region, were populated by both probes. These results suggest that low-energy dipole excitations have underlying structures different from the widely observed isovector giant dipole resonance [1–3]. Comparison with $N = Z$ nuclei, where pure isoscalar dipole excitations are observed, shows that the low-energy dipole excitations in $N > Z$ nuclei also differ from simple isoscalar dipole excitations [6].

Whether the isospin splitting in low-energy dipole excitations is universal among neutron-rich nuclei remains unknown. Of particular interest is the low-energy dipole excitation in unstable nuclei, because recent experimental results point to the enhancement of these excitations in neutron-rich unstable nuclei [1] as compared with stable nuclei in the isotopic chain. However, there is still considerable debate over the mechanism of these excitations [1–3], as well as their systematic behavior in the isotopic chain. To advance the theory and enable a deeper understanding of the mechanism of low-energy dipole excitations in general, it is important to investigate the isospin properties of these excitations in the whole isotopic chain further into the unstable-nuclei region.

In this Letter, the isospin character of low-energy dipole excitations in neutron-rich unstable nucleus ^{20}O was investigated. It is a good nucleus to examine the structure of the low-energy dipole excitation, since four neutrons are added on the doubly magic core of ^{16}O. This nucleus is known to have significantly strong dipole excitations at energies below the neutron threshold [11,12], but only the isovector dipole strength has been determined. Measuring the isoscalar dipole strength of these states is particularly important, since several theories based on collective models [13,14] predict that these states have strong isoscalar dipole strength [14]. By determining both the isoscalar and isovector dipole strength, we should be able to gain more information on the structure of these states.

Our goal was to investigate the isospin character of low-energy dipole excitations in ^{20}O using the same method that was successfully used for stable nuclei to compare two probes with different sensitivities to the isospin. Since the unstable nucleus ^{20}O was produced via projectile fragmentation as a fast beam, in-beam γ-ray spectroscopy was combined with a liquid helium target, used as a dominant isoscalar probe, and a gold target for virtual photon excitation [15], used as a dominant isovector probe. The sensitivity is limited to energies below the neutron separation threshold (7.6 MeV).

2. Experiment

The experiment was performed at Radioactive Isotope Beam Factory (RIBF), operated by RIKEN Nishina Center and the Center for Nuclear Study, University of Tokyo. A ^{48}Ca primary beam was accelerated using a cyclotron complex to an energy of 345 MeV/nucleon with an average intensity of 250 particle nA. The primary beam impinged on a 15-mm-thick beryllium target to produce a secondary ^{20}O beam via a projectile fragmentation reaction. The secondary beam was analyzed and identified event-by-event by the fragment separator BigRIPS [16], using the TOF-ΔE-$B\rho$ method [17]. The properties achieved for the ^{20}O beam were 45% purity, 1.3×10^5 particle/s intensity, and 276(9) MeV/nucleon kinetic energy. The ^{20}O beam impinged on two different reaction targets, a 2.45(5) mm gold target and a 317(28) mg/cm^2 liquid helium target [18]. The liquid helium target system is composed of a cylindrical cell with 10-μm-thick Havar foils as entrance and exit windows. The cell is surrounded by a radiation shield whose windows consist of 7-μm-thick aluminum foils. The reaction products were analyzed by the ZeroDegree spectrometer [16] using the same TOF-$B\rho$-ΔE method. In addition, a low-pressure multi-wire drift chamber [19] was used with standard detectors [16] for particle identification of the reaction products. Decay γ rays from the reaction products were detected by a large-volume $LaBr_3$:Ce scintillator array [20] located at a laboratory angle of 30°. The energy resolution in FWHM was 1.60% at 6.31 MeV. The efficiency was 0.90% for the full-energy peak of 1.84-MeV γ rays emitted from a ^{88}Y calibration source. The efficiency was reproduced within 2.0% precision by a Monte Carlo simulation code built with GEANT4 [21].

3. Analysis

Doppler-corrected γ-ray single spectra are presented in Fig. 1(a) (^{20}O + α) and (c) (^{20}O + Au) in black dots with statistical error bars. In order to suppress the background, the spectra were gated by the time of flight from the targets to the $LaBr_3$:Ce scintillators. The achieved time-of-flight resolution was 610 ps in FWHM. A comparison of the spectra from the two reactions reveals that there are three strong peaks at around 3.68, 5.35, and 6.85 MeV in the ^{20}O + Au spectrum, while these peaks are rather weak in the ^{20}O + α spectrum. This means that these peaks are excited more strongly by the Coulomb potential (gold target) than by the nuclear potential (α target). This target dependence suggests that they are γ rays from the decay of 1^- states. They are consistent with the two 1^- states and their cascade decay via the 2^+_1 state (1.67 MeV) reported in Refs. [11,12], where a lead target was employed for virtual photon excitation. We performed γ–γ coincidence analysis to determine the decay scheme. The γ-ray spectra detected in coincidence with the 2^+_1 state are presented in Fig. 1(b) (^{20}O + α) and (d) (^{20}O + Au). It was confirmed that several peaks in the singles spectra decayed via the 2^+_1 state, and no coincidence with other states was observed within statistical limits.

The spectra were fitted using the least χ^2 method with response functions produced by a Monte Carlo simulation. The response functions were obtained by taking into account the energy of the decay γ rays, placement of the $LaBr_3$:Ce crystals, attenuation of the γ rays by the materials in between the targets and detectors, and velocity of the reaction products emitting the γ rays. As input for the simulation, we employed the established excited states reported in Refs. [11,12] as input for the simulation. In addition, a strong peak was observed at about 3.9 MeV in the γ-ray singles spectra from both reactions, which was also observed in the γ–γ coincidence spectra. The peak was most consistent with a possible 3^- state at 5.62 MeV reported in Ref. [22]. This state was incorporated in the fit as well. Cascade decays via states other

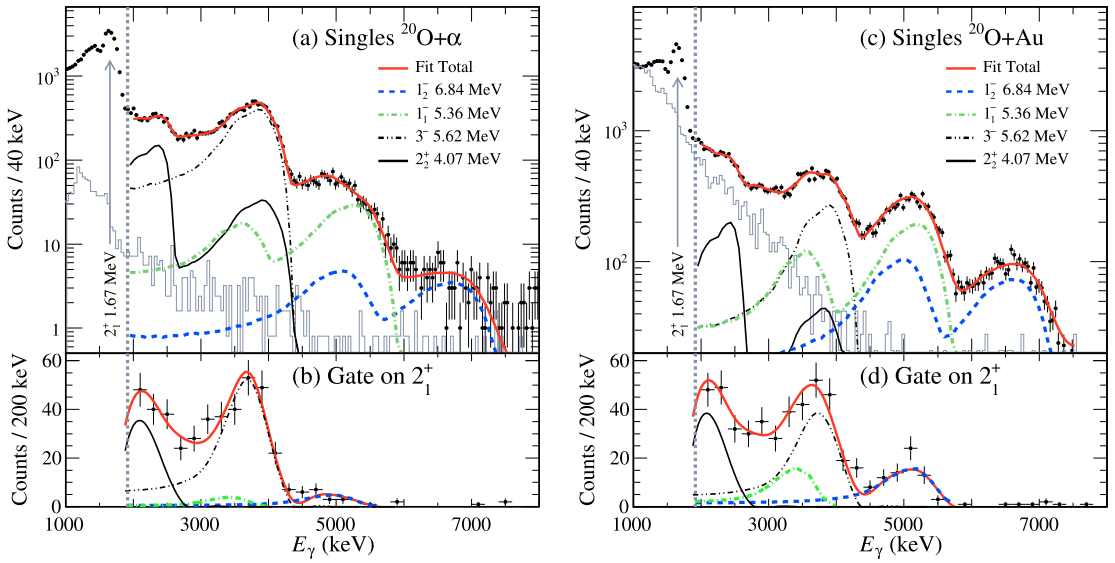

Fig. 1. The Doppler-corrected γ-ray spectra: $^{20}\mathrm{O}+\alpha$ singles (a), $^{20}\mathrm{O}+\alpha$, detected in coincidence with the 2^+_1 state (1.67 MeV) (b), $^{20}\mathrm{O}+\mathrm{Au}$ singles (c), $^{20}\mathrm{O}+\mathrm{Au}$, detected in coincidence with the 2^+_1 state (d). The gray histograms are the background spectra. Error bars are statistical. The fit was performed above the energy of 1900 keV (energy higher than vertical gray-dotted lines).

Table 1
Excited states and decay γ-ray energy, used to produce response functions. E_i and $J^\pi_{n,i}$ indicate the energy and spin-parity of the initial state, while E_f and $J^\pi_{n,f}$ indicate the same for the final state. The values were taken from Refs. [11,12,22,25].

E_i (MeV)	$J^\pi_{n,i}$	E_f (MeV)	$J^\pi_{n,f}$	E_γ (MeV)
1.67[a]	2^+_1	0.00	$0^+_{\mathrm{g.s.}}$	1.67
4.07[a]	2^+_2	1.67	2^+_1	2.40
		0.00	$0^+_{\mathrm{g.s.}}$	4.07
4.46[b]	0^+_2	1.67	2^+_1	2.79
5.00[b]	(3^-)	1.67	2^+_1	3.33
		0.00	$0^+_{\mathrm{g.s.}}$	5.00
5.35[b]	1^-_1	1.67	2^+_1	3.68
		0.00	$0^+_{\mathrm{g.s.}}$	5.35
5.62[c]	(3^-)	1.67	2^+_1	3.94
6.85[b]	1^-_2	1.67	2^+_1	5.18
		0.00	$0^+_{\mathrm{g.s.}}$	6.85

[a] Values from Ref. [26].
[b] Values from Refs. [11,12].
[c] Values from Ref. [22].

than the 2^+_1 state (1.67 MeV) were not considered, since no such decays were identified by the γ–γ coincidence analysis. The decay γ rays used to produce response functions are listed in Table 1. The background spectra obtained from an ^{24}O beam are presented as the gray histograms in Fig. 1(a) and (c). Because no bound excited states are known in ^{24}O [23,24], the spectra are assumed to represent the background. The backgrounds were parametrized for inclusion in the fit. The decay branching ratio of each state to the 2^+_1 state (1.67 MeV) was set as a free parameter in the fit, while the γ-ray energy from each state was fixed. In order to improve the sensitivity to the minimum of χ^2, the histograms for $E_\gamma \geq$ 1.9 MeV (vertical gray dotted line in Fig. 1) were fitted to exclude the high-statistics 2^+_1 state (1.67 MeV). The fits, indicated by the red solid lines in Fig. 1, overall reproduced the spectra well. Although the resolution was limited by Doppler broadening, the fits decomposed two 1^- states from the spectra, as shown by the blue dashed lines (1^-_1; 5.36(5) MeV) and green dash-dotted lines (1^-_2; 6.84(7) MeV). The branching ratios of the 1^- states were determined through γ–γ coincidence analysis. The results are summarized in Table 2.

Table 2
Branching ratios (Br) determined by fitting.

E_i (MeV)	J^π_n	E_f (MeV)	$J^\pi_{n,f}$	Br (%)
5.36(5)	1^-_1	1.67	2^+_1	26(6)
		0.00	$0^+_{\mathrm{g.s.}}$	74(2)
6.84(7)	1^-_2	1.67	2^+_1	48(6)
		0.00	$0^+_{\mathrm{g.s.}}$	52(3)

4. Results

In order to extract the cross sections and transition strengths, a distorted-wave Born approximation (DWBA) analysis was performed by using the Ecis97 code [27]. As nuclear potential, we employed the theoretically developed global optical potential described in Refs. [28–30]. This optical potential, widely used in the analysis of experimental data on unstable nuclei within the suitable energy range, is known to reproduce data well [31].

The cross sections were determined by taking into account the angular distributions of the γ rays and scattering angles of the projectiles, both calculated by the Ecis97 code. In order to account for the effect of the thick gold target, the scattering angle distributions of the projectiles were analyzed in the same way as described in Ref. [31]. The calculated scattering angle distributions were smeared by the average scattering angles from multiple Coulomb scattering in the targets (8 mrad in gold) and by the anglar resolution of the detectors (4 mrad). Then, the experimental cross sections were determined by considering the angular acceptance of the ZeroDegree spectrometer coupled to the smeared scattering angle distributions. For example, in the case of the 2^+_2 (4.07 MeV) state, the angular acceptance of the ZeroDegree spectrometer in the $^{20}\mathrm{O}+\mathrm{Au}$ system was 72%, while that in the $^{20}\mathrm{O}+\alpha$ system was 90%. The experimental cross sections are tabulated in Table 3. The errors considered were the uncertainties related to the statistics, the fits of the γ-ray spectra, the thicknesses of the targets, and the angular acceptance. In the case of the liquid helium target, the contributions from the cell and the heat shield windows were taken into account as well.

Table 3
Measured cross sections in millibarns.

E_x (MeV)	J^π_n	$\sigma(^{20}\mathrm{O}+\alpha)$	$\sigma(^{20}\mathrm{O}+\mathrm{Au})$
4.07(4)	2^+_2	1.11(16)	5.10(62)
5.36(5)	1^-_1	0.376(43)	7.92(35)
5.62(5)	(3^-)	3.10(28)	7.10(55)
6.84(7)	1^-_2	0.079(13)	5.42(35)

In order to confirm if the potential model yields a consistent value with the literature value, we first calculated the transition strength $B(E2)\uparrow$ of the 2^+_2 (4.07 MeV) state, employing the macroscopic vibrational form factor by following the prescription in [32]. While converting the measured cross sections into the $B(E2)\uparrow$ strength, both the Coulomb and nuclear contributions were included via the two deformation parameters, namely, the nuclear deformation β_{2n} and the Coulomb deformation β_{2c}. The two deformation parameters were determined sush as to reproduce consistently the measured cross section from each reaction. The contribution of β_{2c} to the cross section for the $^{20}\mathrm{O}+\mathrm{Au}$ system was 48%, while that for the $^{20}\mathrm{O}+\alpha$ system was 2%. The Coulomb deformation β_{2c} was then converted into the $B(E2)\uparrow$ strength by using the model-dependent relationship $B(E\lambda)\uparrow = (3Ze\beta_{\lambda c}R_c^\lambda/4\pi)^2$ [33], where the R_c is a Coulomb radius. $B(E2)\uparrow$ was found to be $28.8\pm6.6\ e^2\mathrm{fm}^4$. The result is consistent with $B(E2)\uparrow = 30\ e^2\mathrm{fm}^4$ reported in Refs. [11,12], indicating that this potential model is sufficiently reliable for our purpose.

Furthermore, the spin-parity assignment of a possible 3^- state at 5.62 MeV was tested by deducing the transition strength $B(E3)\uparrow$. We used the same method as for the 2^+ state, employing the macroscopic vibrational form factor. The two deformation parameters β_{3n} and β_{3c} were tuned to reproduce the two measured cross sections. But since the Coulomb contribution to the cross section is less than 1% even in the $^{20}\mathrm{O}+\mathrm{Au}$ system, neither probe is sensitive to the Coulomb deformation β_{3c}. In order to determine $B(E3)\uparrow$, we assumed a simple relationship: $\beta_{3n}R_n = \beta_{3c}R_c$, where R_n is a nuclear radius. The strength calculated for the $^{20}\mathrm{O}+\alpha$ system was $B(E3)\uparrow = 1.30(12)\times10^3\ e^2\mathrm{fm}^6$, and for the $^{20}\mathrm{O}+\mathrm{Au}$ system, $B(E3)\uparrow = 1.19(10)\times10^3\ e^2\mathrm{fm}^6$. The two values are averaged to yield a $B(E3)\uparrow$ value of $1.24(8)\times10^3\ e^2\mathrm{fm}^6$. This result is also consistent with the 3^- strength in oxygen isotopes at similar excitation energy: $B(E3)\uparrow = 1.49(7)\times10^3\ e^2\mathrm{fm}^6$ in $^{16}\mathrm{O}$ at 6.13 MeV [34] and $B(E3)\uparrow = 1.30(4)\times10^3\ e^2\mathrm{fm}^6$ in $^{18}\mathrm{O}$ at 5.10 MeV [35]. This strongly suggests the 5.62 MeV state to be 3^-.

The transition strengths of the 1^- states were determined in the same manner, by including both the Coulomb and nuclear contributions in either system, but under the assumption that the Coulomb potential contributed only to the isovector dipole strength and the nuclear potential contributed only to the isoscalar dipole strength. The strength was calculated in units of $B(E1)\uparrow$ ($e^2\mathrm{fm}^2$) for the isovector dipole strength, and isoscalar dipole energy-weighted sum rule (ISD EWSR) fractions (%) for the isoscalar dipole strength [3,4]. The Harakeh–Dieperink dipole form factor [4] was employed to determine the isoscalar dipole strength. The strengths were determined so that the experimental cross sections from both the $^{20}\mathrm{O}+\alpha$ and $^{20}\mathrm{O}+\mathrm{Au}$ systems were reproduced by the same isoscalar and isovector dipole strengths.

The estimated multipole strengths are listed in Table 4. The result for the 1^-_1 (5.36(5) MeV) state of $B(E1)\uparrow = 3.57(20)\times10^{-2}$ $e^2\mathrm{fm}^2$ is 60% smaller than the $B(E1)\uparrow$ value of $6.2(16)\times10^{-2}$ $e^2\mathrm{fm}^2$ reported in Refs. [11,12], while the result for the 1^-_2 (6.84(7) MeV) state ($B(E1)\uparrow = 3.79(26)\times10^{-2}\ e^2\mathrm{fm}^2$) is consistent with the reported $B(E1)\uparrow$ value of $3.5(9)\times10^{-2}\ e^2\mathrm{fm}^2$. The discrepancy in the 1^-_1 state is most likely due to the 3^- state at 5.62 MeV, newly incorporated in the present fit.

Table 4
Estimated multipole strength.

E_x (MeV)	J^π_n	ISD EWSR (%)	$B(E\lambda)\uparrow$ ($e^2\mathrm{fm}^{2\lambda}$)
4.07(4)	2^+_2		28.8 ± 6.6
5.36(5)	1^-_1	2.70(32)	$3.57(20)\times10^{-2}$
5.62(5)	(3^-)		$1.19(10)\times10^3$
6.84(7)	1^-_2	0.67(12)	$3.79(26)\times10^{-2}$

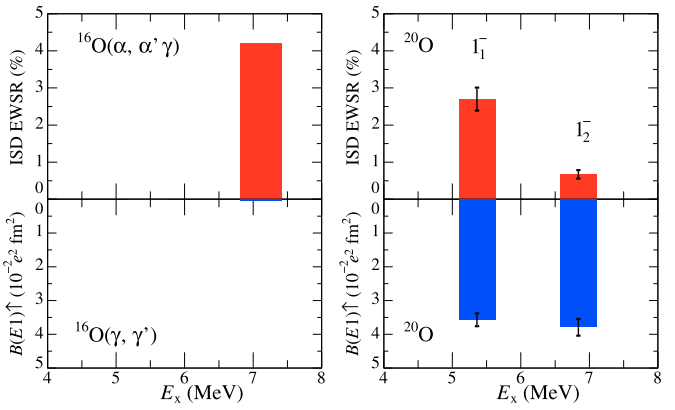

Fig. 2. Measured ISD EWSR (top) and $B(E1)\uparrow$ (bottom) strength in $^{20}\mathrm{O}$ (right panel), in comparison with $^{16}\mathrm{O}$ (left panel).

5. Discussions

The estimated ISD EWSR fractions and $B(E1)\uparrow$ strengths of $^{20}\mathrm{O}$ are plotted in Fig. 2 (right panel), along with the $^{16}\mathrm{O}$ values (left panel) in the same energy region. The $^{16}\mathrm{O}$ ISD EWSR fraction is from Ref. [4], and the $B(E1)\uparrow$ strength is from Ref. [36]. There is a significant difference in $B(E1)\uparrow$ strength between $^{16}\mathrm{O}$, the doubly magic nucleus in the oxygen chain, and $^{20}\mathrm{O}$. The $B(E1)\uparrow$ strength integral over the two states ($\Sigma B(E1)\uparrow$) is increased from $0.492\times10^{-2}\ e^2\mathrm{fm}^2$ in $^{16}\mathrm{O}$ to $7.36(33)\times10^{-2}\ e^2\mathrm{fm}^2$ in $^{20}\mathrm{O}$. More interestingly, the integrated ISD EWSR fraction (ΣISD EWSR) does not show much variation: 4.2% in $^{16}\mathrm{O}$ and 3.37(34)% in $^{20}\mathrm{O}$. In the case of $^{16}\mathrm{O}$, because it is $N=Z$, the isovector dipole strength is strongly suppressed. This explains the almost purely isoscalar nature of the state referred to as the macroscopic squeezing mode [3,4], but the present results indicate that low-energy dipole excitations in $^{20}\mathrm{O}$ exhibit a dual character, suggesting that these states have different underlying structures.

The experimental results were compared with the random-phase approximation (RPA) calculation using SLy4 and SkI2 Skyrme interactions [37]. The properties of the 1^- states predicted by RPA below the neutron-separation threshold are tabulated in Table 5. The transition density calculated by using the SLy4 interaction is plotted in Fig. 3. In contrast to previous theoretical studies [13,14], which mainly predicted the neutron contribution, RPA predicted that the excitation mostly involved the one-particle-one-hole state of the proton. This leads to a rather strong isovector with weaker isoscalar strength. The relationship between the isovector and isoscalar strengths was similar to that observed for the 1^-_2 state at 6.84(7) MeV, regardless of the interaction. Meanwhile, another 1^-_1 state at 5.36(5) MeV had a much stronger isoscalar strength that hardly compared to the prediction. Thus, we deduce the 1^-_2 state at 6.84(7) MeV is generated by the proton excitation, leading to its dominant isovector character. The other 1^-_1 state at 5.36(5) MeV hardly explained by the present RPA may originate from more complex effects. One possibility is that this 1^-_1 state cannot be represented by the superposition of the one-particle-one-hole excitations, on which the present RPA is built. In

Table 5
RPA calculation results.

Interaction	E_x (MeV)	ISD EWSR (%)	$B(E1)\uparrow$ (e^2fm^2)
SkI2	6.51	0.43	3.49×10^{-2}
SLy4	5.52	0.22	1.02×10^{-2}

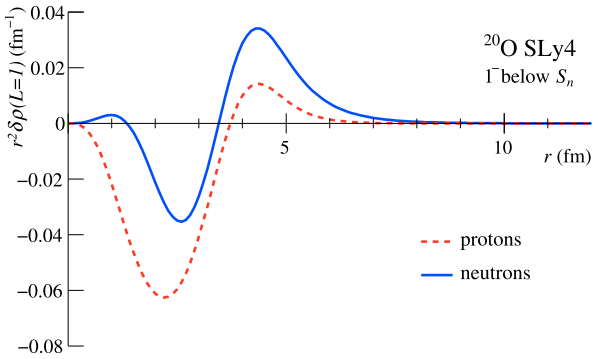

Fig. 3. The transition density of the 1^- state below the neutron-separation threshold calculated by RPA. Protons are represented by the dashed red line and neutrons by the solid blue line. (For interpretation of the references to color in this figure legend, the reader is referred to the web version of this article.)

this scenario, more elaborate calculation considering two-particle–two-hole states is desired. Another possibility is the paring correlation. In this case, the valence neutrons may contribute to the 1^-_1 state, because the paring correlation affects the orbital occupancy of the valence neutrons. Further theoretical studies considering these effects are called for to reveal the structure of this 1^-_1 state.

It is also interesting to compare the low-energy dipole strengths with those in other neutron-rich nuclei. The low-energy dipole strengths in mid-to-heavy-region neutron-rich nuclei listed in Ref. [2] show that there is a similar trend among neutron-rich nuclei: The isoscalar dipole strength decreases with increasing energy, while the isovector dipole strength is largely unchanged below the neutron threshold. When we compare the two low-energy dipole excitations in ^{20}O, the first even-even neutron-rich unstable nuclei in the oxygen chain, we find that the two states show the same trends in strength. Since the comparison with RPA suggests that the proton excitation generates the dominant isovector character, investigating such state in various neutron-rich nuclei is possibly important to understand the isovector-dominant part of this tendency. For the understanding of the other part of the tendency with both isoscalar and isovector strengths, further theoretical studies are necessary.

6. Summary

In summary, the isospin character of low-energy dipole excitations in ^{20}O was investigated for the first time in unstable nuclei by comparing inelastic α scattering as a dominant isoscalar probe and virtual photon scattering as a dominant isovector probe. Two known low-energy 1^- states were populated not only by virtual photons, but also by inelastic α scattering. The 1^-_1 state (5.36(5) MeV) had an isoscalar dipole strength of 2.70(32)% in ISD EWSR, while the 1^-_2 state (6.84(7) MeV) had a strength of 0.67(12)% in ISD EWSR. These states, however, have comparable isovector dipole strengths: $B(E1)\uparrow = 3.57(20) \times 10^{-2}$ e^2fm^2 for the 1^-_1 state and $B(E1)\uparrow = 3.79(26) \times 10^{-2}$ e^2fm^2 for the 1^-_2 state. The difference in isoscalar response suggests that these states have different underlying structures. The comparison with RPA calculation suggests the 1^-_2 state derives from the proton excitation, meanwhile the 1^-_1 state possibly originates from more complex effects, such as coupling to the two-particle–two-hole state and the paring correlation.

Acknowledgements

We are grateful to the RIKEN accelerator team for supplying a stable beam. We also thank T. Furumoto for discussions. This work was partially supported by INFN Italy, which provided the large-volume $LaBr_3$:Ce scintillator array. One of the authors (N. N.) thanks the JRA program of RIKEN. This work was partially supported by JSPS KAKENHI Grant Nos. JP19740166 and JP22684011.

References

[1] D. Savran, T. Aumann, A. Zilges, Experimental studies of the Pygmy Dipole Resonance, Prog. Part. Nucl. Phys. 70 (2013) 210, http://dx.doi.org/10.1016/j.ppnp.2013.02.003.
[2] A. Bracco, F.C.L. Crespi, E.G. Lanza, Gamma decay of pygmy states from inelastic scattering of ions, Eur. Phys. J. A 51 (2015) 99, http://dx.doi.org/10.1140/epja/i2015-15099-6.
[3] M.N. Harakeh, A. van der Woude, Giant Resonances, Oxford University Press, 2001.
[4] M.N. Harakeh, A.E.L. Dieperink, Isoscalar dipole resonance: Form factor and energy weighted sum rule, Phys. Rev. C 23 (1981) 2329, http://dx.doi.org/10.1103/PhysRevC.23.2329.
[5] T.D. Poelhekken, S.K.B. Hesmondhalgh, H.J. Hofmann, A. van der Woude, M.N. Harakeh, Low-energy isoscalar dipole strength in ^{40}Ca, ^{58}Ni, ^{90}Zr and ^{208}Pb, Phys. Lett. B 278 (1992) 423, http://dx.doi.org/10.1016/0370-2693(92)90579-S.
[6] V. Derya, D. Savran, J. Endres, M.N. Harakeh, H. Hergert, J.H. Kelley, P. Papakonstantinou, N. Pietralla, V.Yu. Ponomarev, R. Roth, G. Rusev, A.P. Tonchev, W. Tornow, H.J. Wörtche, Isospin properties of electric dipole excitations in ^{48}Ca, Phys. Lett. B 730 (2014) 288, http://dx.doi.org/10.1016/j.physletb.2014.01.050.
[7] D. Negi, M. Wiedeking, E.G. Lanz, E. Litvinova, A. Vitturi, R.A. Bark, L.A. Bernstein, D.L. Bleuel, S. Bvumbi, T.D. Bucher, B.H. Daub, T.S. Dinoko, J.L. Easton, A. Görgen, M. Guttormsen, P. Jones, B.V. Kheswa, N.A. Khumalo, A.C. Larsen, E.A. Lawrie, J.J. Lawrie, S.N.T. Majola, L.P. Masiteng, M.R. Nchodu, J. Ndayishimye, R.T. Newman, S.P. Noncolela, J.N. Orce, P. Papka, L. Pellegri, T. Renstrøm, D.G. Roux, R. Schwengner, O. Shirinda, S. Siem, Nature of low-lying electric dipole resonance excitations in ^{74}Ge, Phys. Rev. C 94 (2016) 024332, http://dx.doi.org/10.1103/PhysRevC.94.024332.
[8] J. Endres, E. Litvinova, D. Savran, P.A. Butler, M.N. Harakeh, S. Harissopulos, R.-D. Herzberg, R. Krücken, A. Lagoyannis, N. Pietralla, V.Yu. Ponomarev, L. Popescu, P. Ring, M. Scheck, K. Sonnabend, V.I. Stoica, H.J. Wörtche, Isospin Character of the Pygmy Dipole Resonance in ^{124}Sn, Phys. Rev. Lett. 105 (2010) 212503, http://dx.doi.org/10.1103/PhysRevLett.105.212503.
[9] J. Endres, D. Savran, A.M. van den Berg, P. Dendooven, M. Fritzsche, M.N. Harakeh, J. Hasper, H.J. Wörtche, A. Zilges, Splitting of the pygmy dipole resonance in ^{138}Ba and ^{140}Ce observed in the $(\alpha, \alpha'\gamma)$ reaction, Phys. Rev. C 80 (2009) 034302, http://dx.doi.org/10.1103/PhysRevC.80.034302.
[10] D. Savran, M. Babilon, A.M. van den Berg, M.N. Harakeh, J. Hasper, A. Matic, H.J. Wörtche, A. Zilges, Nature of the Pygmy Dipole Resonance in ^{140}Ce studied in $(\alpha, \alpha'\gamma)$ experiments, Phys. Rev. Lett. 97 (2006) 172502, http://dx.doi.org/10.1103/PhysRevLett.97.172502.
[11] E. Tryggestad, T. Aumann, T. Baumann, D. Bazina, J.R. Beene, Y. Blumenfeld, B.A. Brown, M. Chartier, M.L. Halbert, P. Heckman, J.F. Liang, D.C. Radford, D. Shapira, M. Thoennessen, R.L. Varner, Low-lying dipole strength in ^{20}O, Phys. Lett. B 541 (2002) 52, http://dx.doi.org/10.1016/S0370-2693(02)02224-4.
[12] E. Tryggestad, T. Baumann, P. Heckman, M. Thoennessen, T. Aumann, D. Bazin, Y. Blumenfeld, J.R. Beene, T.A. Lewis, D.C. Radford, D. Shapira, R.L. Varner, M. Chartier, M.L. Halbert, J.F. Liang, Low-lying E1 strength in ^{20}O, Phys. Rev. C 67 (2003) 064309, http://dx.doi.org/10.1103/PhysRevC.67.064309.
[13] G. Co', V. De Donno, M. Anguiano, A.M. Lallena, Pygmy and giant electric dipole responses of medium-heavy nuclei in a self-consistent random-phase approximation approach with a finite-range interaction, Phys. Rev. C 87 (2013) 034305, http://dx.doi.org/10.1103/PhysRevC.87.034305.
[14] D. Bianco, F. Knapp, N. Lo Iudice, P. Veselý, F. Andreozzi, G. De Gregorio, A. Porrino, A self-consistent study of multipole response in neutron-rich nuclei using a modified realistic potential, J. Phys. G 41 (2014) 025109, http://dx.doi.org/10.1088/0954-3899/41/2/025109.
[15] T. Motobayashi, Y. Ikeda, Y. Ando, K. Ieki, M. Inoue, N. Iwasa, T. Kikuchi, M. Kurokawa, S. Moriya, S. Ogawa, H. Murakami, S. Shimoura, Y. Yanagisawa, T. Nakamura, Y. Watanabe, M. Ishihara, T. Teranishi, H. Okuno, R.F. Casten, Large deformation of the very neutron-rich nucleus ^{32}Mg from intermediate-energy

Coulomb excitation, Phys. Lett. B 346 (1995) 9, http://dx.doi.org/10.1016/0370-2693(95)00012-A.

[16] T. Kubo, D. Kameda, H. Suzuki, N. Fukuda, H. Takeda, Y. Yanagisawa, M. Ohtake, K. Kusaka, K. Yoshida, N. Inabe, T. Ohnishi, A. Yoshida, K. Tanaka, Y. Mizoi, BigRIPS separator and ZeroDegree spectrometer at RIKEN RI Beam Factory, Prog. Theor. Exp. Phys. 2012 (2012) 03C003, http://dx.doi.org/10.1093/ptep/pts064.

[17] N. Fukuda, T. Kubo, T. Ohnishi, N. Inabe, H. Takeda, D. Kameda, H. Suzuki, Identification and separation of radioactive isotope beams by the BigRIPS separator at the RIKEN RI Beam Factory, Nucl. Instrum. Methods Phys. Res., Sect. B 317 (2013) 323, http://dx.doi.org/10.1016/j.nimb.2013.08.048.

[18] H. Ryuto, M. Kunibu, T. Minemura, T. Motobayashi, K. Sagara, S. Shimoura, M. Tamaki, Y. Yanagisawa, Y. Yano, Liquid hydrogen and helium targets for radioisotope beams at RIKEN, Nucl. Instrum. Methods Phys. Res., Sect. A 555 (2005) 1, http://dx.doi.org/10.1016/j.nima.2005.08.102.

[19] H. Miya, S. Ota, T. Fujii, S. Kawase, Y. Kubota, C.S. Lee, H. Matsubara, K. Miki, A. Saito, S. Michimasa, T. Uesaka, H. Sakai, S. Shimoura, Development of low-pressure multi-wire drift chambers for high-resolution spectroscopy with radioactive isotope beams, Nucl. Instrum. Methods Phys. Res., Sect. B 317 (2013) 701, http://dx.doi.org/10.1016/j.nimb.2013.08.018.

[20] A. Giaz, L. Pellegri, S. Riboldi, F. Camera, N. Blasi, C. Boiano, A. Bracco, S. Brambilla, S. Ceruti, S. Coelli, F.C.L. Crespi, M. Csatlòs, S. Frega, J. Gulyàs, A. Krasznahorkay, S. Lodetti, B. Million, A. Owens, F. Quarati, L. Stuhl, O. Wieland, Characterization of large volume $3.5'' \times 8''$ $LaBr_3$:Ce detectors, Nucl. Instrum. Methods Phys. Res., Sect. A 729 (2013) 910, http://dx.doi.org/10.1016/j.nima.2013.07.084.

[21] S. Agostinelli, et al., Geant4—a simulation toolkit, Nucl. Instrum. Methods Phys. Res., Sect. A 506 (2003) 250, http://dx.doi.org/10.1016/S0168-9002(03)01368-8.

[22] M. Wiedeking, S.L. Tabor, J. Pavan, A. Volya, A.L. Aguilar, I.J. Calderin, D.B. Campbell, W.T. Cluff, E. Diffenderfer, J. Fridmann, C.R. Hoffman, K.W. Kemper, S. Lee, M.A. Riley, B.T. Roeder, C. Teal, V. Tripathi, I. Wiedenhöver, p-sd Shell Gap Reduction in Neutron–Rich Systems and Cross–Shell Excitations in ^{20}O, Phys. Rev. Lett. 94 (2005) 132501, http://dx.doi.org/10.1103/PhysRevLett.94.132501.

[23] K. Tshoo, Y. Satou, H. Bhang, S. Choi, T. Nakamura, Y. Kondo, S. Deguchi, Y. Kawada, N. Kobayashi, Y. Nakayama, K.N. Tanaka, N. Tanaka, N. Aoi, M. Ishihara, T. Motobayashi, H. Otsu, H. Sakurai, S. Takeuchi, Y. Togano, K. Yoneda, Z.H. Li, F. Delaunay, J. Gibelin, F.M. Marqués, N.A. Orr, T. Honda, M. Matsushita, T. Kobayashi, Y. Miyashita, T. Sumikama, K. Yoshinaga, S. Shimoura, D. Sohler, T. Zheng, Z.X. Cao, N = 16 Spherical Shell Closure in ^{24}O, Phys. Rev. Lett. 109 (2012) 022501, http://dx.doi.org/10.1103/PhysRevLett.109.022501.

[24] C.R. Hoffman, T. Baumann, D. Bazin, J. Brown, G. Christian, D.H. Denby, P.A. DeYoung, J.E. Finck, N. Frank, J. Hinnefeld, S. Mosby, W.A. Peters, W.F. Rogers, A. Schiller, A. Spyrou, M.J. Scott, S.L. Tabor, M. Thoennessen, P. Voss, Evidence for a doubly magic ^{24}O, Phys. Lett. B 672 (2009) 17, http://dx.doi.org/10.1016/j.physletb.2008.12.066.

[25] C.R. Hoffman, B.B. Back, B.P. Kay, J.P. Schiffer, M. Alcorta, S.I. Baker, S. Bedoor, P.F. Bertone, J.A. Clark, C.M. Deibel, B. DiGiovine, S.J. Freeman, J.P. Greene, J.C. Lighthall, S.T. Marley, R.C. Pardo, K.E. Rehm, A. Rojas, D. Santiago-Gonzalez, D.K. Sharp, D.V. Shetty, J.S. Thomas, I. Wiedenhöver, A.H. Wuosmaa, Experimental study of the ^{19}O(d, p)^{20}O reaction in inverse kinematics, Phys. Rev. C 85 (2012) 054318, http://dx.doi.org/10.1103/PhysRevC.85.054318.

[26] D.R. Tilley, C.M. Cheves, J.H. Kelley, S. Raman, H.R. Weller, Energy levels of light nuclei, A = 20, Nucl. Phys. A 636 (1998) 249, http://dx.doi.org/10.1016/S0375-9474(98)00129-8.

[27] J. Raynal, Recurrence relations for distorted-wave Born approximation Coulomb excitation integrals and their use in coupled channel calculations, Phys. Rev. C 23 (1981) 2571, http://dx.doi.org/10.1103/PhysRevC.23.2571.

[28] T. Furumoto, W. Horiuchi, M. Takashina, Y. Yamamoto, Y. Sakuragi, Global optical potential for nucleus-nucleus systems from 50 MeV/u to 400 MeV/u, Phys. Rev. C 85 (2012) 044607, http://dx.doi.org/10.1103/PhysRevC.85.044607.

[29] T. Furumoto, Y. Sakuragi, Y. Yamamoto, Effect of repulsive and attractive three-body forces on nucleus–nucleus elastic scattering, Phys. Rev. C 80 (2009) 044614, http://dx.doi.org/10.1103/PhysRevC.80.044614.

[30] T. Furumoto, Y. Sakuragi, Y. Yamamoto, New complex G-matrix interactions derived from two- and three-body forces and application to proton–nucleus elastic scattering, Phys. Rev. C 78 (2008) 044610, http://dx.doi.org/10.1103/PhysRevC.78.044610.

[31] K. Li, Y. Ye, T. Motobayashi, H. Scheit, P. Doornenbal, S. Takeuchi, N. Aoi, M. Matsushita, E. Takeshita, D. Pang, H. Sakurai, Relativistic Coulomb excitation in ^{32}Mg near 200 MeV/nucleon with a thick target, Phys. Rev. C 92 (2015) 014608, http://dx.doi.org/10.1103/PhysRevC.92.014608.

[32] P.G. Thirolf, B.V. Pritychenko, B.A. Brown, P.D. Cottle, M. Chromik, T. Glasmacher, G. Hackman, R.W. Ibbotson, K.W. Kemper, T. Otsuka, L.A. Riley, H. Scheit, Spectroscopy of the 2_1^+ state in ^{22}O and shell structure near the neutron drip line, Phys. Lett. B 485 (2000) 16, http://dx.doi.org/10.1016/S0370-2693(00)00720-6.

[33] S. Raman, C.W. Nestor JR., P. Tikkanen, Transition probability from the ground to the first-excited 2+ state of even-even nuclides, At. Data Nucl. Data Tables 78 (2001) 1, http://dx.doi.org/10.1006/adnd.2001.0858.

[34] H. Lancman, A.P.M. van 'T Westende, H. Graber, Strengths of isospin forbidden E1 transitions in ^{40}Ca and ^{16}O, Nucl. Phys. A 291 (1977) 293, http://dx.doi.org/10.1016/0375-9474(77)90321-9.

[35] D.M. Manley, B.L. Berman, W. Bertozzi, T.N. Buti, J.M. Finn, F.W. Hersman, C.E. Hyde-Wright, M.V. Hynes, J.J. Kelly, M.A. Kovash, S. Kowalski, R.W. Lourie, B. Murdock, B.E. Norum, B. Pugh, C.P. Sargent, D.J. Millener, Electroexcitation of negative-parity states in ^{18}O, Phys. Rev. C 43 (1991) 2147, http://dx.doi.org/10.1103/PhysRevC.43.2147.

[36] C.P. Swann, Widths of the 6.92 MeV and 7.12 MeV levels of 16O, Nucl. Phys. A 150 (1970) 300, http://dx.doi.org/10.1016/0375-9474(70)90953-X.

[37] T. Inakura, H. Imagawa, Y. Hashimoto, S. Mizutori, M. Yamagami, K. Matsuyanagi, Mixed representation RPA calculation for octupole excitations on superdeformed states in the ^{40}Ca and neutron-rich sulfur regions, Nucl. Phys. A 768 (2006) 61, http://dx.doi.org/10.1016/j.nuclphysa.2006.01.008.